Formation of Population II Star Clusters in the Aftermath of a Pair Instability Supernova

Muhammad A. Latif[1] and Dominik Schleicher[2]

[1] Physics Department, College of Science, United Arab Emirates University, P.O. Box 15551, Al-Ain, UAE; latifne@gmail.com
[2] Astronomy Department, Universidad de Concepción, Barrio Universitario, Concepción, Chile
Received 2020 July 26; revised 2020 September 30; accepted 2020 October 1; published 2020 October 19

Abstract

Population II (Pop II) stars formed a few hundred million years after the Big Bang were key drivers of cosmic reionization and building blocks of high-redshift galaxies. How and when these stars formed is a subject of ongoing research. We conduct cosmological radiation hydrodynamical simulations to investigate the formation of Pop II star clusters in dark matter halos forming at $z = 10$–25 in the aftermath of a pair instability supernova (PISN). Our simulations model the formation of Population III and Pop II stars in a self-consistent manner along with their radiative, chemical, and SN feedback in halos of 5×10^5–$7 \times 10^7 \, M_\odot$. We find that a PISN evacuates the gas from halos $\leqslant 3 \times 10^6 \, M_\odot$ and thereafter shuts off in situ star formation for at least 30 Myr. Pop II stellar clusters of $923 \, M_\odot$ and $6800 \, M_\odot$ form in halos of $3.8 \times 10^7 \, M_\odot$ and $9 \times 10^7 \, M_\odot$, respectively. The mode of star formation is highly episodic and mainly regulated by Pop II SN feedback. The average star formation rates are 10^{-5}–$10^{-4} \, M_\odot \, \mathrm{yr}^{-1}$, and the star formation efficiency is less than 1%.

Unified Astronomy Thesaurus concepts: Population III stars (1285); Population II stars (1284); Supernovae (1668); Cosmology (343); Star formation (1569); Star forming regions (1565); High-redshift galaxies (734)

1. Introduction

High-redshift surveys have observed more than 800 galaxies within the first billion years after the Big Bang including candidate galaxies up to $z \sim 11$ (Bouwens et al. 2016; Oesch et al. 2016; Lam et al. 2019; Bowler et al. 2020). These surveys have shifted the observational frontier up to the cosmic dawn. High-redshift galaxies observed at $z \sim 10$ are potential hosts of the first stellar populations, key drivers of cosmic reionization and metal enrichment in the universe. The questions of how and when these galaxies formed stars have stimulated a lot of theoretical interest, and the upcoming James Webb Space Telescope is expected to further unveil properties of their stellar populations.

The first stars known as Population III (Pop III) stars are presumed to be formed in dark matter halos of 10^5–$10^6 \, M_\odot$ at $z = 20$–30. Baryonic collapse in these minihalos is triggered by molecular hydrogen that can cool the gas down to 200 K in the absence of metals and lead to the formation of Pop III stars. The numerical simulations of Pop III stars suggest a wide range of possible masses from 1 to $1000 \, M_\odot$ (Abel et al. 2000; Bromm et al. 2002; Clark et al. 2011; Latif et al. 2013; Stacy et al. 2016; Riaz et al. 2018; Sugimura et al. 2020). These metal-free stars are hotter than the present-day stars, produce copious amounts of radiation, and photoionize the gas clouds in the surrounding medium (Schaerer 2002; Whalen & Norman 2008; Whalen et al. 2013). They either go off as a pair instability supernova (PISN) for a stellar mass between 140 and $260 \, M_\odot$, or SN II if the mass ranges from 11 to $40 \, M_\odot$. For masses above $260 \, M_\odot$ they directly collapse into a black hole.

In the aftermath of SNe, metal lines, and dust grains cool the gas down to the cosmic microwave background temperature above a critical metallicity of $\sim 3 \times 10^{-4} \, Z_\odot$, leading to the formation of Population II (Pop II) stars (Schneider et al. 2003; Omukai et al. 2005; Glover & Jappsen 2007; Wise et al. 2012a; Bovino et al. 2014; Latif et al. 2016). The process of metal enrichment is highly inhomogeneous (Chen et al. 2017; Hartwig & Yoshida 2019) and can be external through SN winds (Smith et al. 2015) or via fallback of metal-rich gas (Ritter et al. 2015; Chiaki & Wise 2019). Various studies have explored the impact of dust cooling suggesting that it can operate at an even lower metallicity of $\sim 10^{-5} \, Z_\odot$ (Dopcke et al. 2011, 2013; Bovino et al. 2016). Safranek-Shrader et al. (2014) performed simulations employing sink particles and evolved one of the clumps for 7000 yr at a fixed metallicity of $10^{-2} \, Z_\odot$. They found that a star cluster of subsolar up to a few solar masses is formed. Smith et al. (2015) explored the impact of dust cooling in an externally metal-enriched halo, and recently Chiaki & Wise (2019) investigated the impact of fallback from a core-collapse SN by modeling dust/metal yields. These studies found that rapid dust cooling at high densities can lead to the formation of metal-poor stars.

While metal enrichment and metal-poor star formation have been explored to some degree, the important question if and how a Pop II star cluster may form after a PISN so far has not been answered. PISNe are about 100 times more powerful than SNe II and have much higher metal yields. They may unbind low-mass halos and impact the gas dynamics. It is not clear how massive Pop II stellar clusters have formed in the first atomic cooling halos and what their properties have been.

In this study we explore the formation of Pop II stellar clusters in the aftermath of a PISN. We self-consistently model the formation of Pop III and Pop II stars along with their radiative, chemical, and mechanical feedback in cosmological simulations. We employ the radiative transfer module MORAY coupled with hydrodynamics to model UV feedback from each Pop III and Pop II star particle. In total, we perform five cosmological radiation hydrodynamical simulations of halos with mass ranging from 5×10^5–$7 \times 10^7 \, M_\odot$ at a maximum physical resolution of 2000 au. Our simulations follow the evolution for about 80 Myr after the formation of the first Pop III star and provide estimates of Pop II cluster masses in these halos. In Section 2, we present our simulation setup. We present our findings in Section 3 and discuss our conclusions in Section 4.

2. Numerical Method

Simulations are carried out using the cosmological hydrodynamics code Enzo (Bryan et al. 2014) coupled with the radiative transfer module MORAY (Wise & Abel 2011) to model radiative feedback from stars. We employ the MUSIC package (Hahn & Abel 2011) to generate cosmological initial conditions at $z = 150$ with a root grid resolution of 256^3 and further employ two nested grid refinement levels in a computational periodic box of size $1\,\mathrm{Mpc\,h}^{-1}$. We make use of the *must refine particle* approach to add refinement in the Lagrange volume of 2 times the viral radius of the halo. Each dark matter (DM) particle is further split into 13 daughter particles in the region of interest, and this approach yields an effective DM resolution of $\sim 5\,M_\odot\,\mathrm{h}^{-1}$. We further employ 13 additional refinement levels during the course of the simulations that result in a physical spatial resolution of about 2000 au. Our refinement criteria are based on particle mass resolution, the baryonic overdensity, and the Jeans refinement of at least 16 cells (Latif & Khochfar 2019).

In total, we have simulated five halos of 5×10^5–$9 \times 10^7\,M_\odot$, at $z = 26$, $z = 20$, $z = 15$, $z = 13.6$, and $z = 12.5$, respectively. We turn on star formation in the halo soon after reaching the maximum refinement level and simultaneously switch on both radiative and SN feedback. Our recipes for star formation and stellar feedback are based on Wise & Abel (2008) and Wise et al. (2012b) and similar to Latif et al. (2018) and Latif & Khochfar (2020). A Pop III star particle is created when a cell meets the following criteria: (1) an overdensity of 5×10^5 ($10^3\,\mathrm{cm}^{-3}$ at $z = 10$, II) and an H_2 fraction of $\geqslant 5 \times 10^{-4}$ (III) convergent flow. The requirement of a minimum H_2 fraction ensures that Pop III stars form in molecular clouds. Each Pop III star particle represents a single star whose mass is randomly sampled from the Salpeter-type initial mass function with a mass range from 1 to $300\,M_\odot$. In our simulation, we are unable to resolve an individual Pop II star due to the computational constraints, and therefore a single Pop II star particle represents a small cluster of stars. Our criteria for Pop II stars are similar to the ones for Pop III without the requirement of a minimum H_2 fraction and they are distinguished based on the metallicity. Pop II stars are allowed to form in cells with $T < 1000\,\mathrm{K}$ and a minimum metallicity of $10^{-4}\,Z_\odot$.

The radiative feedback from stars (both Pop III and Pop II) is modeled using the ray-tracing module MORAY (Wise & Abel 2011) self-consistently linked with hydrodynamics. Pop III and Pop II stars are considered monochromatic sources of radiation with photon energies of 29.6 eV and 21.6 eV, respectively. For Pop III stars, we take the mass-dependent ionizing and Lyman–Werner luminosities from Schaerer (2002) while Pop II stars emit 2.4×10^{47} photons^{-1} s^{-1} $M_\odot^{-1}$ (Schaerer 2003). For SN feedback from Pop III stars, we consider both PISN and type II SN for stellar masses between 140 and $260\,M_\odot$ and 11–$40\,M_\odot$, respectively. Pop II stars generate 6.8×10^{48} erg s^{-1} $M_\odot^{-1}$ after 4 Myr. The SN energy for both Pop III and Pop II stars is distributed in the surrounding 3^3 cells, and all stars forming in a sphere of 1 pc are merged to reduce the amount of ray-tracing. Pop II stars live for 20 Myr corresponding to the lifetime of an OB star. For further details see Wise et al. (2012b). Our chemical model solves the nonequilibrium time-dependent rate equations of primordial species (H, H$^+$, H$^-$, He, He$^+$, He^{++}, H$_2$, H$_2^+$, e$^-$) based on Abel et al. (1997) and is coupled with MORAY. It includes various cooling and heating processes for primordial
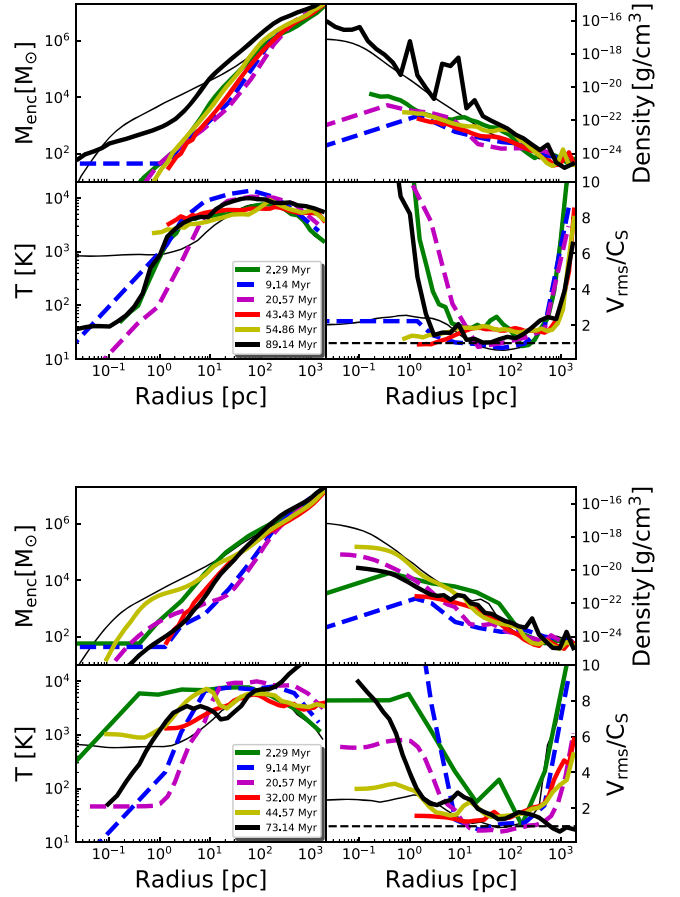

Figure 1. The time evolution of the averaged radial profiles of density, temperature, enclosed gas mass, and turbulent velocity for halo 1 (top panel) and halo 2 (bottom panel) after the formation of a Pop III star is shown here. The thin solid line shows the state of the simulation at the onset of SF. After 2.2 Myr a Pop III star dies a PISN and a Pop II star cluster begins to form within a few Myr. They evacuate the gas from the halo center, drive outflows, and turbulence.

chemistry, metallicity-dependent metal line cooling from Glover & Jappsen (2007) in the temperature regime of 100–$10^4\,\mathrm{K}$, and above $10^4\,\mathrm{K}$ cooling from Sutherland & Dopita (1993). We consider a background flux of strength unity in units of $J_{21} = 10^{-21}$ erg cm^{-2} s^{-1} Hz^{-1} Sr^{-1}.

3. Results

In total, we have simulated five halos of masses $9 \times 10^7\,M_\odot$, $3.8 \times 10^7\,M_\odot$, $5 \times 10^5\,M_\odot$, $1 \times 10^6\,M_\odot$, and $3.0 \times 10^6\,M_\odot$, named as halo 1, halo 2, halo 3, halo 4, and halo 5, respectively. We follow the gravitational collapse in these halos until the central gas cloud is sufficiently cooled via H_2 and collapsed to the densities of 10^{-18} g cm^{-3}. Star formation in the halo is activated at this stage and a Pop III star of $182\,M_\odot$ forms at the center of each halo. The radiative feedback from the Pop III star is modeled with the 3D radiation transport algorithm MORAY coupled to hydrodynamics for about 2.2 Myr corresponding to its lifetime. Radiation from the star photoionizes the surrounding gas and photodissociates H_2. A H II region develops around the star and the density drops down to 10^{-25} g cm^{-3}. At the end of its life, the star dies as PISN and deposits $E_{\mathrm{PISN}} = 3.6 \times 10^{52}$ erg into the halo. Consequently, halos 3, 4, and 5 (below $10^7\,M_\odot$) are evaporated as the energy deposition from PISN exceeds their binding energy.
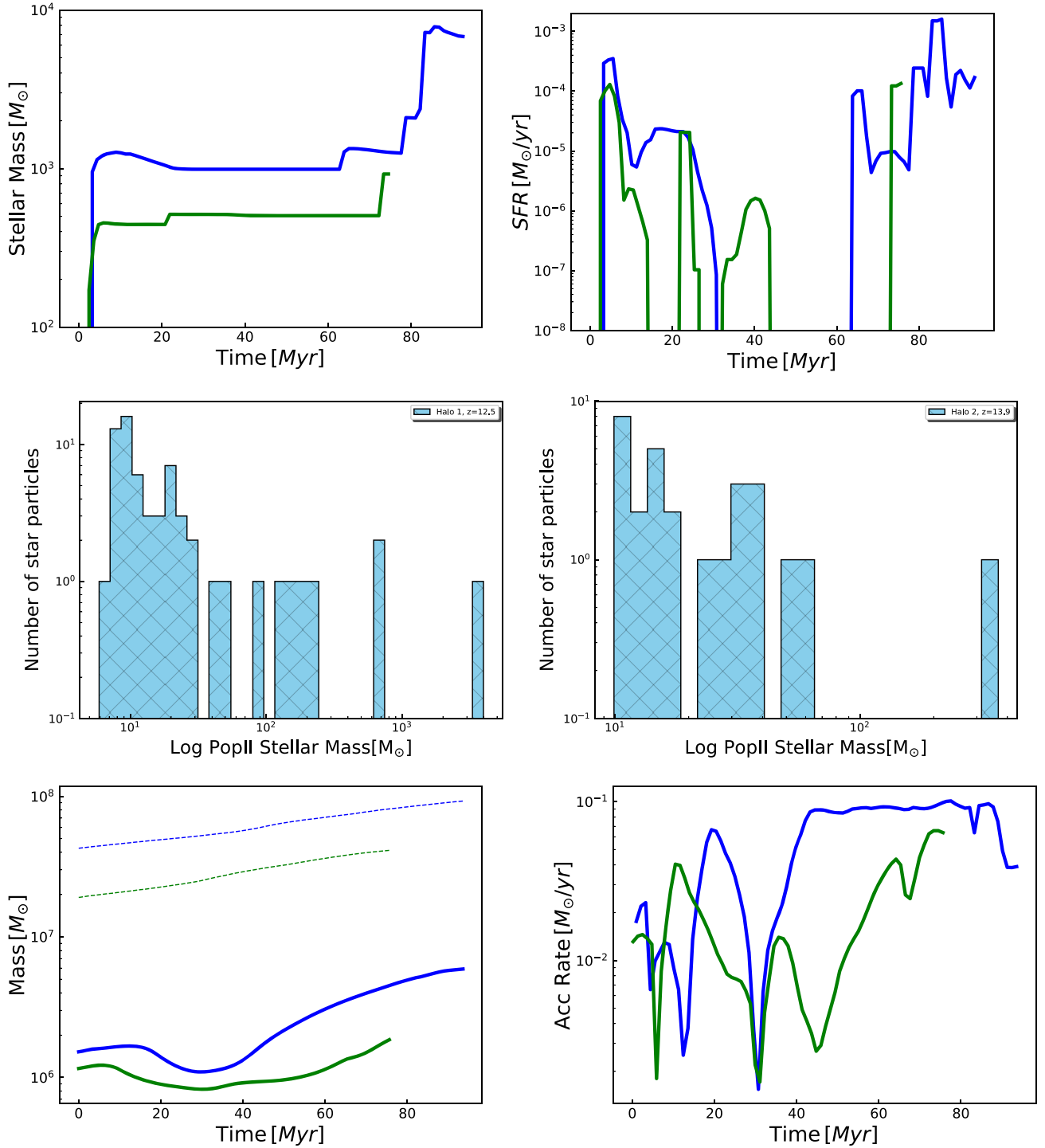
Figure 2. The time evolution of stellar mass and SFR in halos 1 and 2 (top panels), the mass distribution of Pop II star particles (middle panels), and gas mass and mass accretion rate into the central 300 pc (bottom panels). The blue line corresponds to halo 1, the green line halo 2, and the dashed lines correspond to the total halo mass.

Subsequently, we evolved these halos and found that star formation shuts off for at least 31 Myr. Therefore, we hereafter discuss star formation in the rest of the two halos with masses larger than $10^7 M_\odot$.

In halos 1 and 2, after the death of a Pop III star as a PISN, dense cold clumps are formed by metal cooling in the SN ejecta. They result in a starburst within 2 Myr leading to the formation of Pop II star clusters of $954 M_\odot$ and $450 M_\odot$ in halos 1 and 2, respectively. The radiative feedback from Pop II

stars heats the gas in their vicinity and dissociates the cold dense gas. After 4 Myr, feedback from Pop II SNe further heats and evacuates the gas from the halo center. Consequently, the density drops below 10^{-24} g cm^{-3} in the central 10 pc, the temperature increases to a few thousand K, and cold dense gas gets depleted. Star formation remains halted for a few Myr and even up to about 20 Myr on one occasion. In Figure 1 we show profiles of density, enclosed gas mass, temperature, and turbulent Mach number for halo 1 and halo 2, respectively.
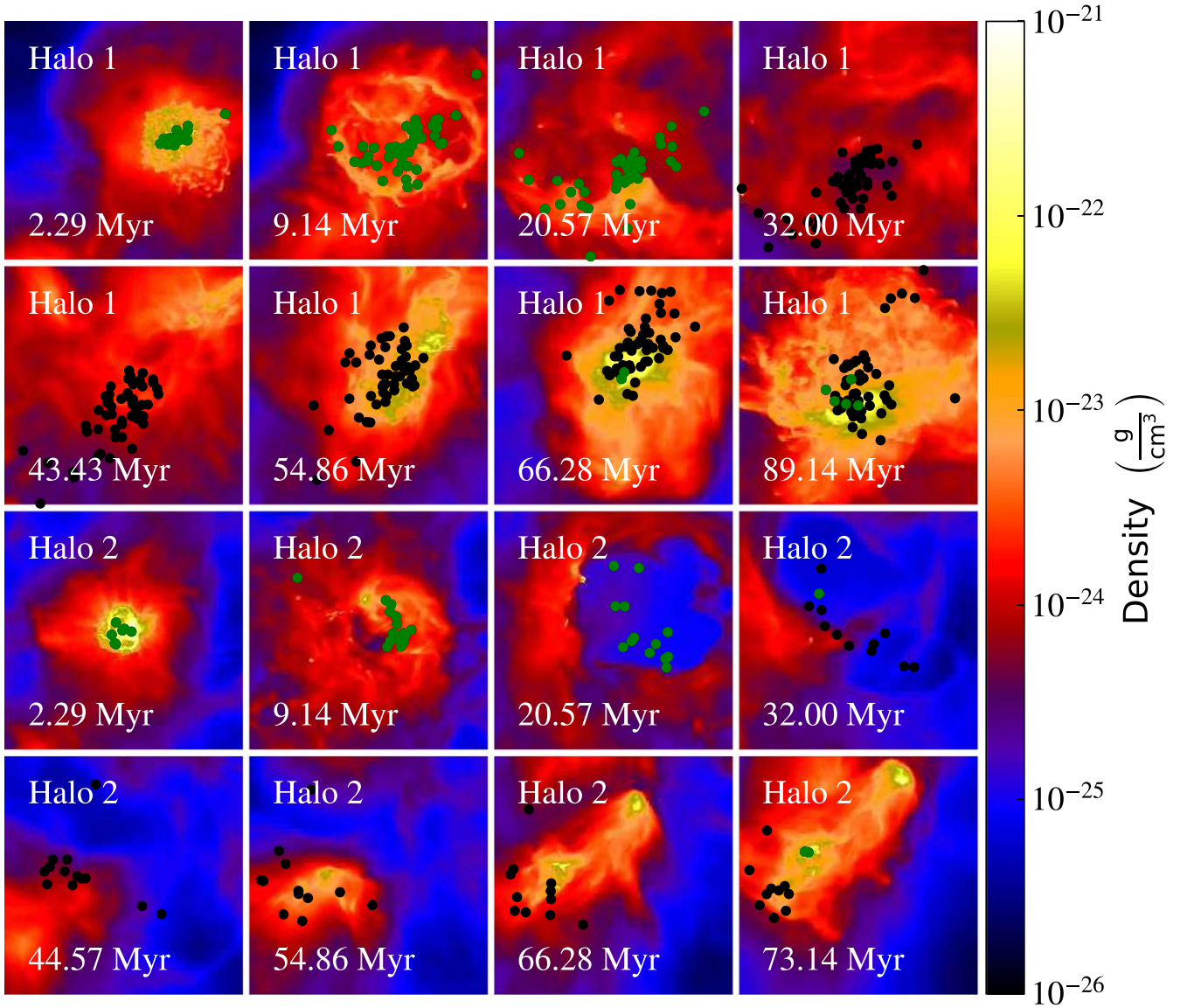
Figure 3. Time evolution of the density distribution in halo 1 and halo 2 for the central 500 pc after the formation of a Pop III star. The green and black points represent young (ages <20 Myr) and old (ages >20 Myr) Pop II stars.

The density varies from 10^{-24}–10^{-17} g/cm$^-$, and bumps in the density profile indicate the presence of dense clumps. The temperature in the center cools down to 30 K in the central 10 pc and is a few thousand K above 10 pc due to the longer cooling time at lower densities of 10^{-24}–10^{-23} g cm^{-3}. The time evolution of gas density and temperature shows the evacuation and heating of the gas in the halo center. The gas mass distribution in the central 10 pc is severely effected by SN feedback and decreases by two orders of magnitude. In halo 1 the mass profile is recovered after 70 Myr, but in halo 2 the gas mass in the central 10 pc is about an order of magnitude lower. The typical turbulent Mach number in the central 10 pc is larger than 1, suggesting that turbulence is supersonic.

The time evolution of stellar mass and star formation rates (SFRs) for halo 1 and 2 are shown in Figure 2. In halo 1, the initial increase in the stellar mass is due to the starburst in the aftermath of a PISN that results in $\sim$1000 $M_\odot$. Stellar mass continues to increase, reaches 1236 $M_\odot$, and a small decline is due to the mass loss via SNe. The stellar mass remains constant for the next 50 Myr as SNe evacuate the gas from the halo

center and no significant SF occurs in halo 1 for 60 Myr. The jump in the stellar mass at 60 Myr is due to the formation of massive star particles. At 78 and 82 Myr massive star particles of 849 $M_\odot$ and 4857 $M_\odot$ form in the cold dense clumps that boost the stellar mass to $\sim$7220 $M_\odot$. They lose 40 $M_\odot$ and 900 $M_\odot$ due to SNe, respectively. The total stellar mass in halo 1 by the end of simulation is $\sim$6800 $M_\odot$. The star formation history shows that the mode of star formation is bursty and mainly regulated by SN feedback alongside significant contributions from radiative feedback. There are epochs such as those between 40 and 60 Myr when SF completely shuts down due to the depletion of cold star-forming gas. In the last 20 Myr, the stellar mass is increased by a factor of 4. SFR varies from 10^{-6}–10^{-3} $M_\odot$ yr^{-1}, and the average SFR in halo 1 is about $\sim$10^{-4} $M_\odot$ yr^{-1}. Similar to halo 1, the initial starburst in halo 2 yields a stellar mass of 443 $M_\odot$ that remains almost constant until 70 Myr, 10 Myr longer than in halo 1 except for a short starburst at 20 Myr. No star formation activity is observed between 50 and 70 Myr due to the lack of cold gas supply regulated by SNe. At 75 Myr the increase in stellar mass to
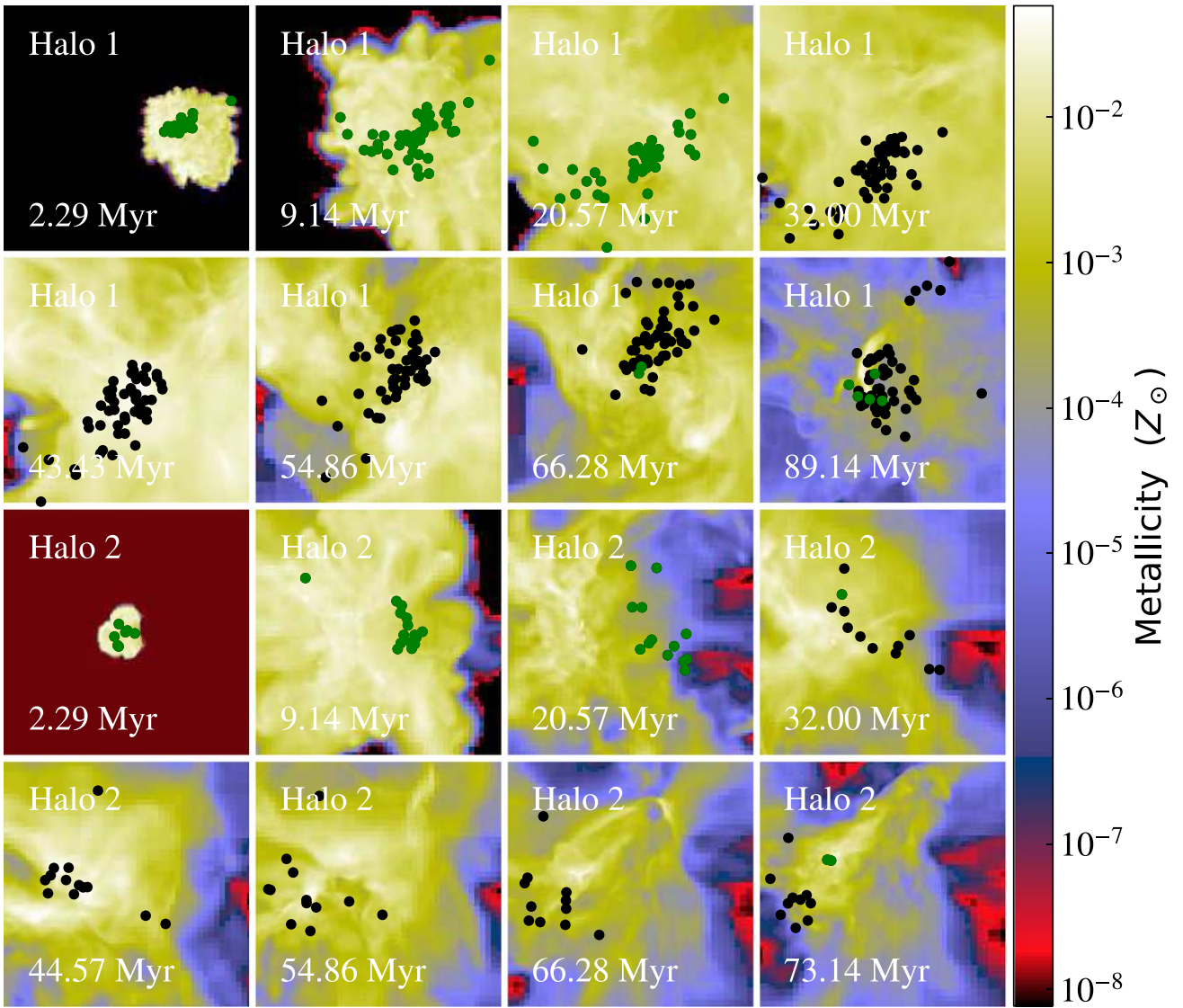
Figure 4. Time evolution of the metallicity distribution in the central 500 pc, same as Figure 3.
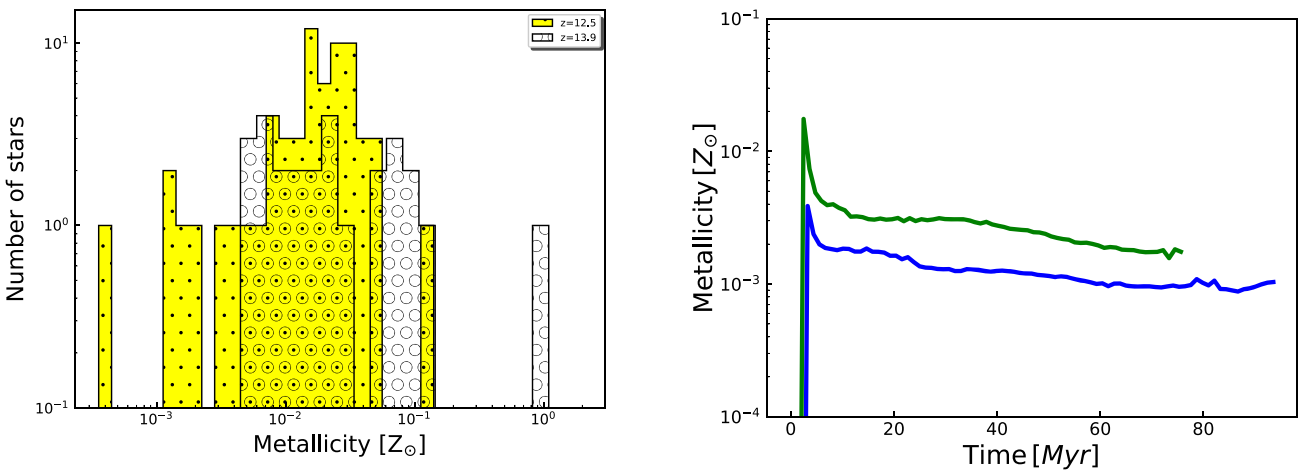

Figure 5. The metallicity distribution of Pop II star particles (left) and the average metallicity of the halos (right).

$923\,M_\odot$ is due to the formation of star particles of $366\,M_\odot$, $38\,M_\odot$, and $14\,M_\odot$. The star formation history of halo 2 shows that SF occurs in short bursts and the SFR varies from 10^{-7}–$10^{-4}\,M_\odot\,\mathrm{yr}^{-1}$. The mean SFR in halo 2 is $1.2 \times 10^{-5}\,M_\odot\,\mathrm{yr}^{-1}$. Overall, halo 2 is more prone to SN feedback due to its shallower DM potential. Compared to halo 1, the

average SFR in halo 2 is 10 times lower and the stellar mass a factor of 7.3 smaller.

The total gas mass in halo 1 and halo 2 is $\sim 10^7\,M_\odot$ and $5 \times 10^6\,M_\odot$, respectively, but only a small fraction of less than 1% is turned into stars. In Figure 3 we show the time evolution of the star particle distribution overplotted on gas density in both halos. At the onset of Pop II star formation, the density distribution is more concentrated, but the radiative and SNe feedback from stars expels the gas and redistributes it in the halo. Consequently, the mean gas density decreases down to $10^{-25}\,\mathrm{g\,cm^{-3}}$ in the center and the fallback leads to an enhanced SFR during the last 20 Myr in the case of halo 1. The average metallicity in both halos is shown in Figure 4; initially the metallicity is mainly concentrated in the halo center and spreads through the halo due to the turbulent mixing over time. The average metallicity in both halos is $\sim 10^{-2}\,Z_\odot$. Overall the metal distribution is inhomogeneous, but the metal fraction in the dense gas is above the critical value. Hence, no Pop III stars form. The same trend is observed for both halos. The mass distribution of star particles is shown in Figure 2. In total, we have 66 star particles in halo 1, most of them are in the mass range of 5–30 $M_\odot$, six are between 100 and 200 $M_\odot$, and only one has a mass of 3969 $M_\odot$. In halo 2, there are 27 star particles in total, only one is 366 $M_\odot$, while most of them have masses between 10 and 40 $M_\odot$. The massive star particles are formed in the cold dense clumps. They represent a small cluster of stars instead of a single massive star.

We have evolved the simulations for 92 Myr and 74 Myr after the formation of the first Pop III star in halos 1 and 2, respectively. The gas masses at the end of the simulations in halos 1 and 2 are $1.4 \times 10^7\,M_\odot$ and $5 \times 10^6\,M_\odot$. The gas mass in halo 1 is doubled in about 80 Myr, while in halo 2 it is increased by a factor of 1.5. This suggests that the growth of halo 1 is faster than for halo 2. The gas mass in the central 300 pc for halo 1 and halo 2 is $6 \times 10^6\,M_\odot$ and $1.8 \times 10^6\,M_\odot$. The mass accretion rate onto the central 300 pc (where most of the star formation occurs) during the first 40 Myr is $\sim 0.02\,M_\odot\,\mathrm{yr^{-1}}$ for both halos; see Figure 2. For halo 1 it increased up to $\sim 0.1\,M_\odot\,\mathrm{yr^{-1}}$, while for the halo 2 it is $\sim 0.06\,M_\odot\,\mathrm{yr^{-1}}$. We also compared the accretion timescale ($M_\mathrm{gas}/M_\mathrm{in}\,\mathrm{yr^{-1}}$) with the mass-loss time ($M_\mathrm{gas}/M_\mathrm{out}\,\mathrm{yr^{-1}}$) at the virial radius of the halo and find that the accretion time is about a factor of 10 shorter than the mass-loss time for halo 1, but for halo 2 they are comparable. The mass-depletion time (M_gas/SFR) for both halos is about 10 Gyr. Assuming that 1% of the total gas in the halo turns into stars over time, we expect these clusters to grow up to $10^5\,M_\odot$ and $5 \times 10^4\,M_\odot$.

The metallicity distribution of Pop II stars ranges from 0.001 to 0.1 $Z_\odot$ with an average value of a few times 0.01 $Z_\odot$; see Figure 5. This is an order of magnitude higher than the metallicity of stars forming from type II SNe (Jeon et al. 2015). Our results show that the average metallicity in halos 1 and 2 is a few times $\geqslant 0.001\,Z_\odot$, and Pop II SF is suppressed in halos of $< 10^7\,M_\odot$ in agreement with previous studies (Wise et al. 2012b; Muratov et al. 2013; Jeon et al. 2014). Our estimates of SFRs and stellar masses are a factor of a few lower in comparison with the previous studies due to the energetics of a PISN (Jeon et al. 2015; Kimm et al. 2016).

4. Conclusions

Our results show that a PISN expels the gas from halos $\leqslant 3 \times 10^6\,M_\odot$ and shuts off SF for at least 31 Myr. Halos with mass $> 10^7\,M_\odot$ can retain gas and Pop II stars form in SN ejecta regulated by metal cooling. SF occurs in episodes and is mainly regulated by Pop II SN feedback in tandem with radiative feedback. The mean SFR is 10^{-5}–$10^{-4}\,M_\odot\,\mathrm{yr^{-1}}$, and the star formation efficiency is $\leqslant 1\%$. Star clusters of 923 $M_\odot$ and $\sim 6800\,M_\odot$ form in halos of $3.8 \times 10^7\,M_\odot$ and $9 \times 10^7\,M_\odot$. The average metallicity in the halos is a few times $\sim 10^{-3}\,Z_\odot$ well above the critical metallicity; consequently, Pop III star formation shuts off in the host halos.

ORCID iDs

Muhammad A. Latif ⓘ https://orcid.org/0000-0003-2480-0988
Dominik Schleicher ⓘ https://orcid.org/0000-0002-9642-120X

References

Abel, T., Anninos, P., Zhang, Y., & Norman, M. L. 1997, NewA, 2, 181
Abel, T., Bryan, G. L., & Norman, M. L. 2000, ApJ, 540, 39
Bouwens, R. J., Oesch, P. A., Labbé, I., et al. 2016, ApJ, 830, 67
Bovino, S., Grassi, T., Schleicher, D. R. G., & Banerjee, R. 2016, ApJ, 832, 154
Bovino, S., Grassi, T., Schleicher, D. R. G., & Latif, M. A. 2014, ApJL, 790, L35
Bowler, R. A. A., Jarvis, M. J., Dunlop, J. S., et al. 2020, MNRAS, 493, 2059
Bromm, V., Coppi, P. S., & Larson, R. B. 2002, ApJ, 564, 23
Bryan, G. L., Norman, M. L., O'Shea, B. W., et al. 2014, ApJS, 211, 19
Chen, K.-J., Whalen, D. J., Wollenberg, K. M. J., Glover, S. C. O., & Klessen, R. S. 2017, ApJ, 844, 111
Chiaki, G., & Wise, J. H. 2019, MNRAS, 482, 3933
Clark, P. C., Glover, S. C. O., Smith, R. J., et al. 2011, Sci, 331, 1040
Dopcke, G., Glover, S. C. O., Clark, P. C., & Klessen, R. S. 2011, ApJL, 729, L3
Dopcke, G., Glover, S. C. O., Clark, P. C., & Klessen, R. S. 2013, ApJ, 766, 103
Glover, S. C. O., & Jappsen, A.-K. 2007, ApJ, 666, 1
Hahn, O., & Abel, T. 2011, MNRAS, 415, 2101
Hartwig, T., & Yoshida, N. 2019, ApJL, 870, L3
Jeon, M., Bromm, V., Pawlik, A. H., & Milosavljević, M. 2015, MNRAS, 452, 1152
Jeon, M., Pawlik, A. H., Bromm, V., & Milosavljević, M. 2014, MNRAS, 444, 3288
Kimm, T., Cen, R., Rosdahl, J., & Yi, S. K. 2016, ApJ, 823, 52
Lam, D., Bouwens, R. J., Coe, D., et al. 2019, arXiv:1903.08177
Latif, M. A., & Khochfar, S. 2019, MNRAS, 490, 2706
Latif, M. A., & Khochfar, S. 2020, MNRAS, 497, 3761
Latif, M. A., Omukai, K., Habouzit, M., Schleicher, D. R. G., & Volonteri, M. 2016, ApJ, 823, 40
Latif, M. A., Schleicher, D. R. G., Schmidt, W., & Niemeyer, J. 2013, ApJL, 772, L3
Latif, M. A., Volonteri, M., & Wise, J. H. 2018, MNRAS, 476, 5016
Muratov, A. L., Gnedin, O. Y., Gnedin, N. Y., & Zemp, M. 2013, ApJ, 772, 106
Oesch, P. A., Brammer, G., van Dokkum, P. G., et al. 2016, ApJ, 819, 129
Omukai, K., Tsuribe, T., Schneider, R., & Ferrara, A. 2005, ApJ, 626, 627
Riaz, R., Bovino, S., Vanaverbeke, S., & Schleicher, D. R. G. 2018, MNRAS, 479, 667
Ritter, J. S., Sluder, A., Safranek-Shrader, C., Milosavljević, M., & Bromm, V. 2015, MNRAS, 451, 1190
Safranek-Shrader, C., Milosavljević, M., & Bromm, V. 2014, MNRAS, 440, L76
Schaerer, D. 2002, A&A, 382, 28
Schaerer, D. 2003, A&A, 397, 527
Schneider, R., Ferrara, A., Salvaterra, R., Omukai, K., & Bromm, V. 2003, Natur, 422, 869
Smith, B. D., Wise, J. H., O'Shea, B. W., Norman, M. L., & Khochfar, S. 2015, MNRAS, 452, 2822
Stacy, A., Bromm, V., & Lee, A. T. 2016, MNRAS, 462, 1307

Sugimura, K., Matsumoto, T., Hosokawa, T., Hirano, S., & Omukai, K. 2020, ApJL, 892, L14
Sutherland, R. S., & Dopita, M. A. 1993, ApJS, 88, 253
Whalen, D., & Norman, M. L. 2008, ApJ, 673, 664
Whalen, D. J., Even, W., Frey, L. H., et al. 2013, ApJ, 777, 110
Wise, J. H., & Abel, T. 2008, ApJ, 685, 40
Wise, J. H., & Abel, T. 2011, MNRAS, 414, 3458
Wise, J. H., Abel, T., Turk, M. J., Norman, M. L., & Smith, B. D. 2012a, MNRAS, 427, 311
Wise, J. H., Turk, M. J., Norman, M. L., & Abel, T. 2012b, ApJ, 745, 50